NASA/CR- 206687

IN 39-CR
OCIT
1998
046306

GRANT: NAG1-1686

GLOBAL-LOCAL FINITE ELEMENT ANALYSIS FOR
THERMO-MECHANICAL STRESSES IN BONDED
JOINTS

NASA LANGLEY RESEARCH CENTER

PRINCIPAL INVESTIGATOR:

ERDOGAN MADENCI
AEROSPACE AND MECHANICAL ENGINEERING
UNIVERSITY OF ARIZONA
TUCSON, AZ 85721

ANALYSIS OF BONDED COMPOSITE LAMINATES

S. Shkarayev, E. Madenci,

Department of Aerospace and Mechanical Engineering
The University of Arizona
Tucson, AZ 85721

and

C. J. Camarda

Thermal Structures Branch
NASA Langley Research Center
Hampton, VA 23681-0001

Abstract

An analysis of adhesively bonded joints using conventional finite elements does not capture the singular behavior of the stress field in regions where two or three dissimilar materials form a junction with or without free edges. However, these regions are characteristic of the bonded joints and are prone to failure initiation. This study presents a method to capture the singular stress field arising from the geometric and material discontinuities in bonded composites. It is achieved by coupling the local (conventional) elements with global (special) elements whose interpolation functions are constructed from the asymptotic solution.

Introduction

Although bonded joints are a prime means for transferring load in the construction of composite structures, they are potential failure sites due to the presence of geometric and material discontinuities causing high stress concentrations. Reliable predictions of the gross response of the structure cannot be made accurately unless a precise description can be made of the interface through which the transfer of load is achieved. Thus, understanding the nature of

interfacial stresses is critical in designing reliable bonded joints, and efforts to understand the mechanisms needed to improve the strength of the bonded isotropic and composite materials are still continuing. Previous analyses of bonded joints can be categorized as the "shear-lag" and "finite-element" models. An extensive review and in-depth discussion of the previous investigations can be found in articles by Tsai and Morton (1994) and Ding and Kumosa (1994).

Both the shear-lag models and finite-element models with conventional elements fail to capture the singular stress field at the junction of dissimilar materials. Blanchard and Watson (1986) concluded that a finite element analysis of such regions would not guarantee a convergent peak stress even with continued mesh refinement. In order to capture the exact nature of the stress field and to minimize the intensive computations arising from the refinement of the mesh, Barsoum (1988a, 1988b, 1990) introduced an iterative scheme in conjunction with the finite-element analysis without the use of a special (enriched) element. This approach is effective for a bimaterial interface with or without cracks. However, it suffers from the number of iterations required for convergence and the inability to enforce the continuity of traction components across the interface. Also, the rate of convergence and the accuracy of the results are dependent on the material properties and the scaling of the displacements during the iterations. Ding and Kumosa (1994) and Ding et al. (1994) applied this method to determine the singular stress field near the intersection of a bimaterial interface with free edges in adhesive joints. Although they captured the accurate description of the stress field near the junction, the strength of the singularity becomes inaccurate at distances very close to the free surface, where the failure usually initiates. This may be attributed to the limitation of the finite elements utilized in the analysis.

To overcome this type of shortcoming in modeling a crack along a bimaterial interface, Chen (1985) developed an element with appropriate interpolation functions built in to account for the singularity at the crack tip. The unknown stress intensity factors are included explicitly in the expressions for the interpolation functions, and they are determined directly as part of the solution. Recently, Gadi et al. (1995) extended this method to determine the singular stress field

for the crack tip situated at the junction of three dissimilar sectors of material. Based on a similar concept, Kuo and Chen (1993) introduced a hybrid element with appropriate stress fields to investigate the transient thermal stresses in multi-layered regions with finite dimensions. However, both the hybrid and the enriched elements are limited to a specific geometry where the free edges are either perpendicular or parallel to the bimaterial interface, respectively.

In a finite-element analysis of bonded joints, Destuynder et al. (1992) introduced a method to reduce the adhesive layer to a line through the use of asymptotic expansions of analytical solutions for the singular stress field near the geometric and material discontinuities. Also, Lin and Lin (1993) introduced a new element based on the Timoshenko beam theory for modeling the adhesive layer while accounting for the transverse shear and normal stresses in the adherents. However, this element does not account for the singular behavior of stress fields.

The previous analytical and finite-element investigations were primarily concerned with isotropic adherent materials, because the presence of orthotropic materials is not suitable for directly constructing the analytical solution to the singular stress field. An analysis capability is lacking for determining the exact nature of the stress field in composite structures with bonded joints involving two or three dissimilar materials. Therefore, a global finite element with appropriate interpolation functions to capture the correct singular behavior arising from material and geometric discontinuities is developed here and is implemented into a finite element program with conventional elements. This program permits the analysis of various bonded joint configurations with accurate stress distributions in the critical regions and the extraction of the stress intensification parameter or the energy release rate in the presence of a crack. The results from this analysis provide the required parameters for the fracture criterion introduced by Gradin and Groth (1984) in order to estimate the strength of the bonded joint. Also, this program is integrated into the commercially available finite element program ANSYS so that the designer can use the ANSYS pre- and post-processing capabilities and execute the program within the ANSYS environment.

Solution Method

The global-local finite element concept introduced by Mote (1971) is utilized in determining the stress field in regions consisting of a junction of two or three wedge-shaped sectors of orthotropic material with or without free edges (Figure 1). The extension and application of this method were demonstrated by Bradford et al. (1976, 1979, 1984), Dong (1983), and Her (1990). The development of the global element stiffness matrix is similar to that of a conventional (local) element, except for the interpolation functions. In this study, these functions are established by solving for the stress and displacement fields in the regions illustrated in Figure 1. In these regions, each material is assumed to be elastic, homogeneous, and specially orthotropic, with elastic coefficient C_{ij}^k. In reference to the Cartesian coordinates (x, y), the stress-strain relations under plane-strain assumptions are

$$\begin{Bmatrix} \sigma_{xx} \\ \sigma_{yy} \\ \sigma_{xy} \end{Bmatrix}^k = \begin{bmatrix} C_{11} & C_{12} & 0 \\ C_{12} & C_{22} & 0 \\ 0 & 0 & C_{66} \end{bmatrix}^k \begin{Bmatrix} \varepsilon_{xx} \\ \varepsilon_{yy} \\ 2\varepsilon_{xy} \end{Bmatrix}^k \tag{1}$$

where $\sigma_{\alpha\beta}^k$ and $\varepsilon_{\alpha\beta}^k$ are the stress and strain components, respectively. A method is presented in the Appendix that provides an average stiffness matrix for balanced laminates for which the material and reference coordinate systems do not coincide. This average stiffness matrix contains the independent coefficients of a specially orthotropic material. Throughout this study, the sub- or superscript k denotes a specific sector of the region. The interfaces among the adjacent materials, specified by angles θ_i, are assumed to be perfectly bonded, thus requiring the continuity of traction and displacement components along the interfaces.

The explicit forms of the displacement and stress components in the vicinity of the junction are constructed by solving for the displacement equilibrium equations expressed as

$$C_{11}^k u_{x,xx}^k + C_{66}^k u_{x,yy}^k + (C_{12}^k + C_{66}^k)u_{y,xy}^k = 0$$

$$C_{66}^k u_{y,xx}^k + C_{11}^k u_{y,yy}^k + (C_{12}^k + C_{66}^k)u_{x,xy}^k = 0$$

$$\tag{2}$$

As suggested by Williams (1952), representing the displacement components as

$$u_\alpha^k(r,\theta) = r^\lambda G_\alpha^k(\theta) \quad \text{with } \alpha = x, y \tag{3}$$

permits the reduction of Equation (2) to a system of ordinary differential equations in terms of the unknown functions $G_\alpha^k(\theta)$ in matrix form[*]

$$\mathbf{M}_k(\theta; C_{ij})\mathbf{G}_k''(\theta) + (1 - \lambda)\mathbf{M}_k'(\theta; C_{ij})\mathbf{G}_k'(\theta)$$

$$\tag{4}$$

$$-\left[\lambda^2 \mathbf{M}_k(\theta; C_{ij}) + \frac{\lambda}{2}\mathbf{M}_k''(\theta; C_{ij}) - \lambda^2 \mathbf{L}_k(C_{ij})\right]\mathbf{G}_k(\theta) = 0$$

where the known matrices $\mathbf{L}_k$ and $\mathbf{M}_k$ are defined by

$$\mathbf{L}_k(C_{ij}) = \begin{bmatrix} (C_{11}^k + C_{66}^k) & 0 \\ 0 & (C_{22}^k + C_{66}^k) \end{bmatrix}$$

$$\mathbf{M}_k = (\theta; C_{ij}) = \begin{bmatrix} m(\theta; C_{66}^k, C_{11}^k) & \frac{1}{2}m'(\theta; C_{12}^k, C_{66}^k) \\ \frac{1}{2}m'(\theta; C_{12}^k, C_{66}^k) & m(\theta; C_{22}^k, C_{66}^k) \end{bmatrix}$$

with $m(\theta; a, b) = a\cos^2\theta + b\sin^2\theta$. The unknown functions $G_\alpha^k(\theta)$ are contained in the vector $\mathbf{G}_k(\theta)$ as $\mathbf{G}_k^T(\theta) = [G_x^k(\theta), G_y^k(\theta)]$. In Equation (2), the displacement components are defined in reference to a polar coordinate system, (r, θ), whose origin coincides with the junction of the vertices as shown in Figure 1. The unknown parameter λ, dependent on the geometry and the material properties, indicates the strength of the singular behavior for the stress field. Utilizing the displacement representation given in Equation (3) and the strain displacement relations along with Equation 1, the displacement and stress components required for imposing the interface and boundary conditions can be expressed in polar coordinates as

---

[*] Throughout this study, a prime denotes differentiation with respect to the variable θ.

$$\mathbf{u}_k(r,\theta) = r^\lambda \mathbf{T}(\theta) \mathbf{G}_k(\theta)$$

$$\quad (5)$$

$$\boldsymbol{\sigma}_k(r,\theta) = r^{\lambda-1}[\lambda \mathbf{E}_k(\theta; C_{ij}) \mathbf{G}_k(\theta) + \mathbf{F}_k(\theta; C_{ij}) \mathbf{G}'_k(\theta)]$$

in which the explicit forms of the matrices are given by

$$\mathbf{T}(\theta) = \begin{bmatrix} \cos\theta & \sin\theta \\ \sin\theta & \cos\theta \end{bmatrix}$$

$$\mathbf{E}_k(\theta; C_{ij}) = \begin{bmatrix} m(\theta; C_{12}^k, C_{11}^k - 2C_{66}^k)\cos\theta & -m(\theta; C_{22}^k + 2C_{66}^k, C_{12}^k)\sin\theta \\ -m(\theta; C_{11}^k - C_{12}^k - C_{66}^k, C_{66}^k)\cos\theta & m(\theta; C_{66}^k, C_{22}^k - C_{12}^k - C_{66}^k)\sin\theta \end{bmatrix}$$

and

$$\mathbf{F}_k(\theta; C_{ij}) = \begin{bmatrix} -m(\theta; C_{12}^k + 2C_{66}^k, C_{12}^k)\sin\theta & m(\theta; C_{22}^k, C_{12}^k + 2C_{66}^k)\cos\theta \\ m(\theta; C_{66}^k, C_{11}^k - C_{12}^k - C_{66}^k)\cos\theta & -m(\theta; C_{12}^k - C_{22}^k - C_{66}^k, C_{66}^k,)\sin\theta \end{bmatrix}$$

The vectors $\mathbf{u}_k(r,\theta)$ and $\boldsymbol{\sigma}_k(r,\theta)$ contain the displacement and stress components, respectively, as $\mathbf{u}_k^T(r,\theta) = [u_r^k(r,\theta), u_\theta^k(r,\theta)]$ and $\boldsymbol{\sigma}_k^T = [\sigma_{\theta\theta}^T(r,\theta), \sigma_{r\theta}^k(r,\theta)]$. For completeness, the normal stress component, $\sigma_{rr}(r,\theta)$ is given by

$$\sigma_{rr}^k(r,\theta) = r^{\lambda-1}[\lambda \mathbf{e}_k^T(\theta; C_{ij}) \mathbf{G}_k(\theta) + \mathbf{f}_k^T(\theta; C_{ij}) \mathbf{G}'_k(\theta)]$$

where

$$\mathbf{e}_k^T(\theta; C_{ij}) = \begin{bmatrix} m(\theta; C_{11}^k, C_{12}^k + 2C_{66}^k)\cos\theta & m(\theta; C_{12}^k + 2C_{66}^k, C_{22}^k)\sin\theta \end{bmatrix}$$

$$\mathbf{f}_k^T(\theta; C_{ij}) = \begin{bmatrix} -m(\theta; C_{11}^k - 2C_{66}^k, C_{12}^k)\sin\theta & m(\theta; C_{11}^k, C_{22}^k - 2C_{66}^k)\cos\theta \end{bmatrix}$$

Determination of the unknown functions $G_\alpha^k(\theta)$ with $\alpha = x, y$ requires the solution of the system of ordinary differential equations with variable coefficients, Eq. (4), subject to the interface and boundary conditions. In the case of three sectors of dissimilar materials forming a junction, as shown in Figure 1a, the interface conditions are expressed as

$$\left.\begin{array}{ll} \sigma_{\alpha\beta}^{k}(r,\theta_k) = \sigma_{\alpha\beta}^{k+1}(r,\theta_k) & k = 1,2 \\ \\ \sigma_{\alpha\beta}^{k}(r,\theta_k) = \sigma_{\alpha\beta}^{k-2}(r,\theta_{k+1}) & k = 3 \end{array}\right\} \quad \alpha,\beta = r,\theta \text{ with } \alpha = \beta \neq r$$

$$\left.\begin{array}{ll} u_{\alpha}^{k}(r,\theta_k) = u_{\alpha}^{k+1}(r,\theta_k) & k = 1,2 \\ \\ u_{\alpha}^{k}(r,\theta_k) = u_{\alpha}^{k-1}(r,\theta_{k+1}) & k = 3 \end{array}\right\} \quad \alpha,\beta = r,\theta$$

$$(6)$$

For the intersection of a bimaterial interface with free edges, as shown in Figure 1b, the interface and boundary conditions become

$$\left.\begin{array}{l} \sigma_{\alpha\beta}^{k}(r,\theta_k) = 0 \\ \\ \sigma_{\alpha\beta}^{k}(r,\theta_{k+1}) = \sigma_{\alpha\beta}^{k+1}(r,\theta_{k+1}) \\ \\ \sigma_{\alpha\beta}^{k+1}(r,\theta_{k+2}) = 0 \end{array}\right\} \quad k = 1 \text{ and } \alpha,\beta = r,\theta \text{ with } \alpha = \beta \neq r \qquad (7)$$

$$u_{\alpha}^{k}(r,\theta_{k+1}) = u_{\alpha}^{k+1}(r,\theta_{k+1}) \; ; \quad k = 1 \text{ and } \alpha,\beta = r,\theta$$

The solution to the differential equations, Eq. (4), exists for values of λ that satisfy the characteristic equation of the homogeneous system of equations resulting from the imposition of the conditions (Eq. 6 or 7). Because of the complexity of the variable coefficients in Eq. (4), the solution to these equations is constructed numerically by recasting them as a set of first-order ordinary differential equations in terms of $G_{\alpha}^{k}(\theta)$ and $G_{\alpha}'^{k}(\theta)$ in the form

$$\frac{d}{d\theta}\left\{\begin{array}{c} G_x(\theta) \\ G_x'(\theta) \\ G_y(\theta) \\ G_y'(\theta) \end{array}\right\}^{k} = \left[\begin{array}{cccc} 0 & 1 & 0 & 0 \\ A_{11}(\theta;C_{ij},\lambda) & B_{11}(\theta;C_{ij},\lambda) & A_{12}(\theta;C_{ij},\lambda) & B_{12}(\theta;C_{ij},\lambda) \\ 0 & 0 & 0 & 1 \\ A_{21}(\theta;C_{ij},\lambda) & B_{21}(\theta;C_{ij},\lambda) & A_{22}(\theta;C_{ij},\lambda) & B_{22}(\theta;C_{ij},\lambda) \end{array}\right]^{k}\left\{\begin{array}{c} G_x(\theta) \\ G_x'(\theta) \\ G_y(\theta) \\ G_y'(\theta) \end{array}\right\}^{k} \quad (8)$$

where A_{ij} and B_{ij} are the components of the matrices $\mathbf{A}$ and $\mathbf{B}$ defined by

$$\mathbf{A}^{k}(\theta;C_{ij},\lambda) = \mathbf{M}_K^{-1}(\theta;C_{ij})\left[\lambda^2\mathbf{M}_k(\theta;C_{ij}) + \frac{\lambda}{2}\mathbf{M}_k''(\theta;C_{ij}) - \lambda^2\mathbf{L}_k(C_{ij})\right]$$

and

$$\mathbf{B}^k(\theta; C_{ij}, \lambda) = (\lambda - 1)\mathbf{M}_k^{-1}(\theta; C_{ij})\mathbf{M}_k'(\theta; C_{ij})$$

The solution to this form of equations, Eq. (8), subject to the interface and boundary conditions is achieved by a Runge-Kutta forward integration scheme in conjunction with the shooting method. This procedure requires the initial estimates of the eigenvalues, λ, and the corresponding eigenfunctions, $G_\alpha^k(\theta)$, as well as the target conditions. The integration process continues until the target conditions are satisfied, which requires the difference between the computed and prescribed conditions to vanish. In the case of three sectors of dissimilar materials, the target conditions are obtained from the interface conditions between the third and first regions as

$$\mathbf{u}_3(\theta_3) = \mathbf{u}_1(\theta_4) \quad \text{and} \quad \sigma_3(\theta_3) = \sigma_1(\theta_4) \tag{9}$$

with $\theta_4 = 2\pi - \theta_3$. The explicit forms of these conditions are expressed as

$$\mathbf{Q} = \mathbf{G}_3(\theta_3) - \mathbf{G}_1(\theta_4) = 0$$

$$\mathbf{R} = \mathbf{F}_3(\theta_3; C_{ij})\mathbf{G}_3'(\theta_3) + \lambda[\mathbf{E}_3(\theta_3; C_{ij}) - \mathbf{E}_1(\theta_4; C_{ij})]\mathbf{G}_3(\theta_3) - \mathbf{F}_1(\theta_4)\mathbf{G}_1'(\theta_4) = 0 \tag{10}$$

in which $\mathbf{Q}^T = [Q_x, Q_y]$ and $\mathbf{R}^T = [R_x, R_y]$. In order to satisfy these conditions, Eq. (10), a positive definite objective function is defined in terms of the modulus of the complex functions Q_x, Q_y, R_x, and R_y as

$$S = |Q_x|^2 + |Q_y|^2 + |R_x|^2 + |R_y|^2 \tag{11}$$

With the well-established optimization techniques, the objective function is minimized by varying the real and imaginary parts of λ, $\mathbf{G}_1(\theta_4)$, and $\mathbf{G}_1'(\theta_4)$.

Determination of the eigenvalues and corresponding eigenfunctions satisfying the equilibrium equations and the interface conditions permits the expression of stress and displacement components as

$$\sigma_{\alpha\beta} = \sum_{i=1}^{N} x_i \mathcal{F}_{\alpha\beta}(r,\theta;\lambda_i)$$

$$\alpha,\beta = x, y$$

$$u_\alpha = \sum_{i=1}^{N} x_i \mathcal{G}_\alpha(r,\theta;\lambda_i)$$

$$(12)$$

The generalized coefficients, x_i, are determined by enforcing the continuity of the nodal displacements at the interface nodes between the global element and the surrounding local (conventional) elements. As illustrated in Figure 2, the global element with M interface nodes requires the imposition of the continuity conditions given by

$$\begin{Bmatrix} u_x(r_1,\theta_1) \\ u_y(r_1,\theta_1) \\ \vdots \\ u_y(r_M,\theta_M) \\ u_y(r_M,\theta_M) \end{Bmatrix} = \begin{bmatrix} \mathcal{G}_x(r_1,\theta_1;\lambda_1) & \mathcal{G}_x(r_1,\theta_1;\lambda_2) & \cdots & \mathcal{G}_x(r_1,\theta_1;\lambda_N) \\ \mathcal{G}_y(r_1,\theta_1;\lambda_1) & \mathcal{G}_y(r_1,\theta_1;\lambda_2) & \cdots & \mathcal{G}_y(r_1,\theta_1;\lambda_N) \\ \vdots & \vdots & & \vdots \\ \mathcal{G}_x(r_M,\theta_M;\lambda_1) & \mathcal{G}_x(r_M,\theta_M;\lambda_2) & \cdots & \mathcal{G}_x(r_M,\theta_M;\lambda_N) \\ \mathcal{G}_y(r_M,\theta_M;\lambda_1) & \mathcal{G}_x(r_M,\theta_M;\lambda_2) & \cdots & \mathcal{G}_y(r_M,\theta_M;\lambda_M) \end{bmatrix} \begin{Bmatrix} x_1 \\ x_2 \\ \vdots \\ x_N \end{Bmatrix}$$

$$(13)$$

or

$$\{u\} = [\mathcal{G}]\{x\}$$

In general, the number of equations, $2M$, exceeds the number of unknown coefficients, N, resulting in an overdetermined system. Therefore, the unknown coefficients are expressed in terms of nodal displacements based on the least squares minimization procedure as follows:

$$\{x\} = [Z]\{u\} \quad \text{with} \quad [Z] = [[\mathcal{G}]^T[\mathcal{G}]]^{-1}[\mathcal{G}]^T$$

$$(14)$$

Determination of these coefficients permits the expression of the stress and displacement components in terms of the nodal displacements, and the strain energy in the global element becomes[**]

$$U = \frac{1}{2} \int_S \{u\}^T [Z]^T \{\mathcal{F}_{\alpha\beta}\}^T \{\mathcal{G}_\alpha\}[Z]\{u\}\eta_\beta dS \ , \quad \alpha, \beta = x, y \tag{15}$$

where η_β are the components of the unit normal to the surface, S, of the global element. The vectors $\{\mathcal{F}_{\alpha\beta}\}$ and $\{\mathcal{G}_\alpha\}$ are defined as

$$\{\mathcal{F}_{\alpha\beta}\} = \left\{\mathcal{F}_{\alpha\beta}(r,\theta;\lambda_1), \ \mathcal{F}_{\alpha\beta}(r,\theta;\lambda_2), \ ..., \ \mathcal{F}_{\alpha\beta}(r,\theta;\lambda_N)\right\}$$

$$\{\mathcal{G}_\alpha\} = \left\{\mathcal{G}_\alpha(r,\theta;\lambda_1), \ \mathcal{G}_\alpha(r,\theta;\lambda_2), \ ..., \ \mathcal{G}_\alpha(r,\theta;\lambda_N)\right\} \tag{16}$$

Minimizing the strain energy with respect to the nodal displacements associated with the global element results in the global stiffness matrix [k] defined as

$$[k] = \frac{1}{2} \int_S [Z]\{\mathcal{F}_{\alpha\beta}\}^T \{\mathcal{G}_\alpha\} + \{\mathcal{G}_\alpha\}^T \{\mathcal{F}_{\alpha\beta}\})[Z]\eta_\beta dS \tag{17}$$

The global and local element stiffness matrices are assembled to establish the system equilibrium equations as

$$[K]\{\delta\} = \{F\} \tag{18}$$

where $[K]$ is the system stiffness matrix and the vectors $\{\delta\}$ and $\{F\}$ include the total nodal displacement and force components, respectively. This process led to the development of a finite element program incorporating both global and local elements. The local elements consist of quadrilaterals and triangular elements, whose interpolation functions can be found in any textbook on the elementary finite element method. The shape of the global element can be an n-sided polygon, depending on the details of the mesh surrounding the global element. The number of interface nodes and the size of the global element were established based on convergence requirements.

[**] Repeated subscripts imply summation.

This global-local finite element program is implemented in the ANSYS platform through the use of ANSYS Parametric Design Language (APDL) commands. It permits execution of the program without leaving the ANSYS environment. The global element is introduced into the ANSYS element library as "USER104" through the User Programmer Features (UPFs) routines. For this purpose, ANSYS is customized and relinked by including two FORTRAN routines, "uec104.f " and "uel104.f". The first routine describes the characteristics of the element, such as the maximum number of nodes associated with the global element. The second routine arranges the element matrices, load vectors, results, and element solutions data during normal ANSYS execution. However, it acts as a dummy routine because the global-local analysis program is used in constructing the solution rather than ANSYS. The real constants for each global element are defined by:

1. The x and y coordinates of the origin of the local coordinate system associated with the global element.

2. Material number associated with the region.

3. Angle specifying each region.

This capability permits the use of ANSYS pre- and post-processing for the global-local finite element analysis.

Numerical Results

Analysis of bonded dissimilar composite materials by the present approach is demonstrated through a single-lap adhesive joint with three typical configurations. The geometry and dimensions of each of these lap-joint configurations are described in Figure 3. The parameters c_1 and c_2 and h_1 and h_2 denote the end distance (c) and thickness (h) of the top and bottom adherents, respectively, with numerical values of $c_1 = c_2 = 200$ mm and $h_1 = h_2 = 5$ mm. Also, a long and a short joint with overlap lengths of $\ell = 320$ mm and 40 mm are considered in order to capture the effect of joint length. For joint type II, bevel angles of θ_1 and θ_2 are equal and are specified as 45°. The parameters ℓ_1, ℓ_2, ϕ_1, and ϕ_2 describing the

overflow of the adhesive in joint type III are specified as $\ell_1 = \ell_2 = 2h$, with the adhesive thickness $h = 0.4$ mm and $\phi_1 = \phi_2 = 45°$. As shown in Figure 3, the upper adherent is subjected to a uniform stress, σ_0, and the lower adherent is fixed at the other end. The adhesive is an isotropic material with Young's modulus $E = 3400$ MPa and Poisson's ratio $v = 0.35$. Top and bottom adherents are composed of $[0°/90°/0°]$ plies with properties $E_L = 147$ GPa, $E_T = 11$ GPa, $G_{LT} = 5.3$ GPa, and $v_{LT} = 0.3$. The averaged orthotropic properties for the top and bottom adherents are computed to be $118.73 C_{11} =$ GPa, $C_{22} = 36.14$ GPa, $C_{12} = 12.06$ GPa, and $C_{66} = 6.21$ GPa. In the case of isotropic adherents, the Young's modulus and Poisson's ratio are taken as $E = 200$ Gpa and $v = 0.3$, respectively.

The finite element representation of each lap-joint configuration with global and conventional elements is illustrated in Figures 4-6. Their overall deformations under the specified load of $\sigma_0 = 1$ MPa are shown in Figure 7. The eigenvalues retained in the construction of the interpolation functions for each global element are tabulated in Table 1 for the isotropic adherents. For a type I joint, the behavior of the peel and the shear stresses in each global element along the bond line from the junction point is given in Figure 8. The peel and shear stresses along the bond line of the most stressed region represented by global element D for all joint types are shown in Figure 9.

Based on the strain energy density criterion introduced by Sih and Macdonald (1974), an examination of the strain energy density around the junction point for a specified distance provides possible failure sites and the crack propagation path once the failure initiates. The variations of the tangential and shear stresses and the strain energy density for a specified core region, $r_0 = 0.05$ mm, around the junction in each global element are shown in Figures 10-12. These figures reveal that the failure in joint type I is most likely to initiate in global element D at the junction of the top adherent and the adhesive, and it is predicted that it will propagate along the bond line. For type II lap-joints, the possible failure site is also in global element D along the bond line. For type III lap joints, the failure may initiate at the junction points E or F and the

crack is likely to grow into the adhesive in the vertical direction. These results are all based on the eigenvalues presented in Table 1.

Conclusions

The global-local finite element analysis eliminates the use of a fine mesh and provides an accurate description of the stress field in the critical regions of the bonded joints. The order of the singularity along with the corresponding stress intensification parameter can be used for predicting failure in the adhesive layer of the joint. With this capability, the geometry and material properties can be optimized to minimize stress intensification. Also, this approach can be extended to the analysis of bonded joints with visco-elastic adhesive layers. As indicated by Ratwani et al. (1982), the effect of modulus relaxation becomes important because a large redistribution of stresses occurs while the joint is loaded.

References

Barsoum, R. S., 1988a, "Application of the Finite Element Iterative Method to the Eigenvalue Problem of a Crack Between Dissimilar Media," *International Journal for Numerical Methods in Engineering*, Vol. 26, pp. 541-554.

Barsoum, R. S., 1988b, "Theoretical Basis of the Finite Element Iterative Method for the Eigenvalue Problem in Stationary Cracks," *International Journal for Numerical Methods in Engineering*, Vol. 26, pp. 531-539.

Barsoum, R. S., 1990, "Asymptotic Fields at Interfaces Using the Finite Element Iterative Method," *Computers and Structures*, Vol. 35, pp. 285-292.

Blanchard, P. J. and Watson, R. D., 1986, "Residual Stresses in Bonded Armor Tiles for In-Vessel Fusion Components," *Nuclear Engineering and Design*, Vol. 4, pp. 61-66.

Bradford, L. G., Dong, S. B., Nicol, D. A. C., and Westmann, R. A., 1976, "Application of Global-Local Finite Element Method to Fracture Mechanics," Technical Report, EPRI NP-239.

Bradford, L. G., Dong, S. B., Tessler, A., and Westmann, R. A., 1979, "GLASS-II: Global-Local Finite Element Analysis," Technical Report, EPRI NP-1089.

Bradford, L. G., Dong, S. B., Nicol, D. A. C., and Westmann, R. A., 1984, "A Central Crack Element in Fracture Mechanics," *International Journal of Fracture*, Vol. 24, pp. 197-207.

Chen, E. P., 1985, "Finite Element Analysis of a Bimaterial Interface Crack," *Theoretical and Applied Fracture Mechanics*, Vol. 23, pp. 179-188.

Destuynder, P., Micavila, F., Santos, A., and Ousset, Y., 1992, "Some Theoretical Aspects in Computational Analysis of Adhesive Lap Joints," *International Journal for Numerical Methods in Engineering*, Vol. 35, pp. 1237-1262.

Ding, S. and Kumosa, M., 1994, "Singular Stress Behavior at an Adhesive Interface Corner, *Engineering Fracture Mechanics*, Vol. 47, pp. 503-519.

Ding, S., Miikisho, L., and Kumosa, M., 1994, "Analysis of Stress Singular Fields at a Bimaterial Wedge Corner," *Engineering and Fracture Mechanics*, Vol. 47, pp. 569-585.

Dong, S. B., 1983, "Global-Local Finite Element Methods," *State-of-the-Art Surveys in Finite Element Technology* (A. K. Noor and W. D. Pilkey, eds.), ASME, New York, pp. 452-474.

Gadi, K. S., Joseph, P. F., and Kaya, A. C., 1995, "Enriched Finite Elements for a Crack Tip Touching an Interface," *Proceedings of the ASME Winter Annual Meeting*, San Francisco, CA, ASME, New York.

Gradin, P. A. and Groth, H. L., 1984, "A Fracture Criterion for Adhesive Joints in Terms of Material Induced Singularities," *Proceedings of the Third International Conference on Numerical Methods in Fracture Mechanics*, Pineridge Press, Swansea, U.K., pp. 711-720.

Her, S., 1990, "Fracture Mechanics of Interface Cracks Between Dissimilar Anisotropic Materials," PhD dissertation, University of California, Los Angeles.

Kuo, A.-Y. and Chen, K.-L., 1993, "Transient Thermal Stresses in Multilayered Devices," *Thermal Stress and Strain in Microelectronic Packaging* (J. H. Lau, ed.), Van Nostrand Reinhold, New York, pp. 139-172.

Lin, C.-C. and Lin, Y.-S., 1993, "A Finite Element Model of Single-Lap Adhesive Joints," *International Journal of Solids and Structures*, Vol. 30, pp. 1679-1692.

Mote, C. D., Jr., 1971, "Global-Local Finite Element," *International Journal for Numerical Methods in Engineering*, Vol. 3, pp. 565-574.

Ratwani, M. M., Kan, H. P., and Liu, D. D., 1982, "Time-Dependent Adhesive Behavior Effects in a Stepped Lap Joint," *AIAA Journal*, Vol. 20, pp. 734-736.

Sih, G. C. and Macdonald, B., 1974, "Fracture Mechanics Applied to Engineering Problems— Strain Energy Density Fracture Criterion," *Engineering Fracture Mechanics*, Vol. 6, pp. 361-386.

Tsai, M. Y. and Morton, J., 1994, "An Evaluation of Analytical and Numerical Solutions to the Single-Lap Joint," *International Journal of Solids and Structures*, Vol. 31, pp. 2537-2563.

Williams, M. L., 1952, "Stress Singularities Resulting from Various Boundary Conditions in Angular Corners of Plates in Extension," *ASME Journal of Applied Mechanics*, Vol. 19, pp. 526-528.

Appendix

Because only specially orthotropic materials are considered in this formulation, it is limited to laminates with a ply orientation of either 0° or 90°. However, a method exists to determine the average specially orthotropic stiffness matrix for a balanced laminate. A balanced laminate is a panel that has a negatively oriented ply for every positively oriented ply. Thus, this analysis can be expanded to model any balanced laminate if an average stiffness matrix is utilized.

To determine the average stiffness matrix, the stiffness matrix of each ply in the global coordinates is required. The stress-strain relationship for the kth layer of a laminate can be represented as

$$\sigma^k = C^k \varepsilon^k \qquad (19)$$

or

$$\tilde{\sigma}^k = \tilde{C}^k \tilde{\varepsilon}^k \qquad (20)$$

where the tilde denotes the quantities in the local reference frame. The unit vectors of the local reference frame can be written in terms of the direction cosines and the global unit vectors as

$$\begin{Bmatrix} \mathbf{n}_\xi \\ \mathbf{n}_\eta \\ \mathbf{n}_\varsigma \end{Bmatrix}^k = \begin{bmatrix} l_1 & m_1 & n_1 \\ l_2 & m_2 & n_2 \\ l_3 & m_3 & n_3 \end{bmatrix} \begin{Bmatrix} \mathbf{n}_x \\ \mathbf{n}_y \\ \mathbf{n}_z \end{Bmatrix} \qquad (21)$$

With these direction cosines, stresses and strains can be transformed to the global reference frame through the transformation

$$\sigma^k = \mathbf{T}^k \tilde{\sigma}^k$$
$$\varepsilon^k = \mathbf{T}^k \tilde{\varepsilon}^k \qquad (22)$$

where

$$\mathbf{T}^k = \begin{bmatrix} l_1^2 & l_2^2 & l_3^2 & 2l_2 l_3 & 2l_1 l_3 & 2l_1 l_2 \\ m_1^2 & m_2^2 & m_3^2 & 2m_2 m_3 & 2m_1 m_3 & 2m_1 m_2 \\ n_1^2 & n_2^2 & n_3^2 & 2n_2 n_3 & 2n_1 n_3 & 2n_1 n_2 \\ m_1 n_1 & m_2 n_2 & m_3 n_3 & (m_2 n_3 + m_3 n_2) & (m_1 n_3 + m_3 n_1) & (m_1 n_2 + m_2 n_1) \\ l_1 n_1 & l_2 n_2 & l_3 n_3 & (l_2 n_3 + l_3 n_2) & (l_1 n_3 + l_3 n_1) & (l_1 n_2 + l_2 n_1) \\ l_1 m & l_2 m_2 & l_3 m_3 & (l_2 m_3 + l_3 m_2) & (l_1 m_3 + l_3 m_1) & (l_1 m_2 + l_2 m_1) \end{bmatrix} \qquad (23)$$

Substituting Eqs. (21) and (22) into (19) while noting that

$$T^k T^{k^T} = I \qquad (24)$$

yields

$$\sigma^k = T^k \tilde{C}^k T^{k^T} \varepsilon^k \qquad (25)$$

Thus, the transformation of the stiffness matrix from local coordinates to global coordinates is

$$C^k = T^k \tilde{C}^k T^{k^T} \tag{26}$$

The average stiffness matrix, C, of a balanced laminate is then represented by
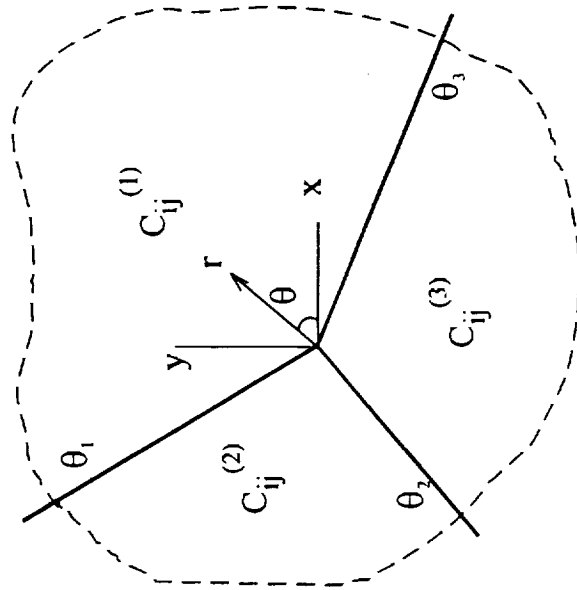
$$C = \frac{1}{h} \sum_1^n t^k C^k \tag{27}$$

which represents an average weighting of the stiffness matrix based on the thickness of the layer. Provided the laminate is balanced, C will represent a specially orthotropic material with 12 nonzero coefficients, 9 of which are independent. This averaging process is expected to provide reasonably acceptable results, provided the paired balancing plies are located closely to one another and the plies are relatively thin.

Table 1. Eigenvalues associated with the global elements in the joints.

Lap-Joint Type	Global Elements		
	A and D	B and C	E and F
Without adhesive overflow	-0.3272 $0.7138 \pm i\,0.5964$	-0.3015 $0.7144 \pm i\,0.5961$	--
Beveled adherents	-0.3272 $0.7138 \pm i\,0.5964$	-0.1604 $0.7053 \pm i\,0.5931$	--
With adhesive overlow	-0.0219 0.1884	-0.0219 0.1814	-0.3702 -0.2211 0.1588 $0.6441 \pm i\,0.0433$

Figure Captions

Figure 1.   Junction of three and two dissimilar orthotropic materials.

Figure 2.   Interface nodes between the global element and the surrounding local elements with or without free edges.

Figure 3.   The geometry of a single lap joint: (a) without adhesive overflow; (b) with beveled adherents; (c) with adhesive overflow.

Figure 4.   Finite element discretization of the lap joint without adhesive overflow.

Figure 5.   Finite element discretization of the lap joint with beveled adherents.

Figure 6.   Finite element discretization of the lap joint with adhesive overflow.

Figure 7.   Overall deformation of the long and short joints.

Figure 8.   Variation of stresses along the interface near the junctions of a short and long joint without adhesive overflow in global elements A-D.

Figure 9.   Variation of stresses along the interface in global element D near the junction of short joints of type I-III.

Figure 10. Variations of the tangential and shear stresses and the strain energy density around the junctions of short joints without adhesive overflow.
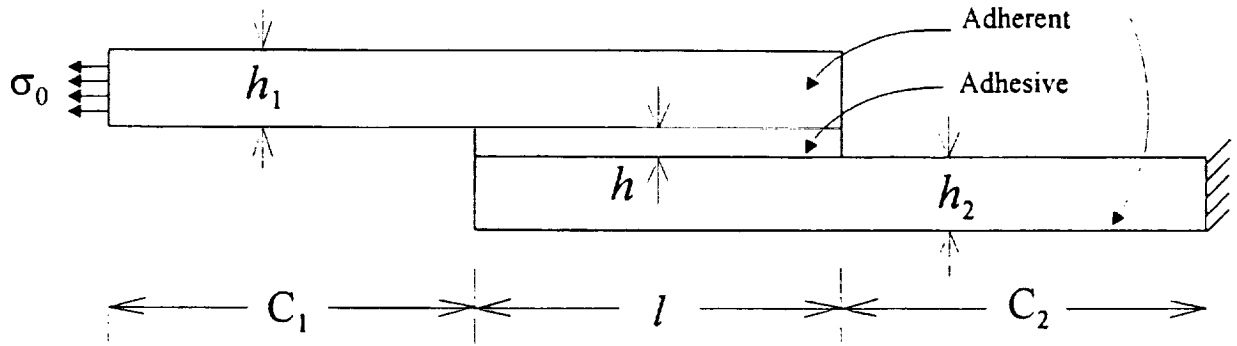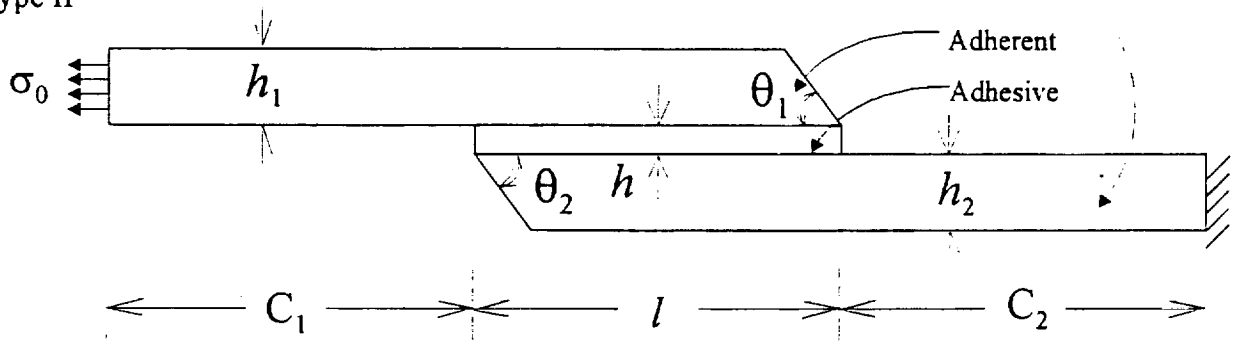
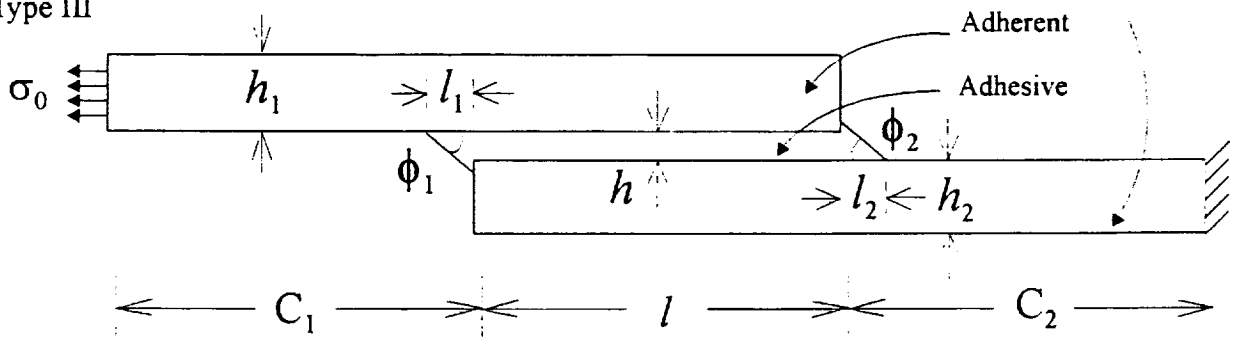Figure 12. Variations of the tangential and shear stresses and the strain energy density around the junctions of short joints with beveled adherents.

Figure 13. Variations of the tangential and shear stresses and the strain energy density around the junctions of short joints with adhesive overflow.

$C_{ij}^{(2)}$

$C_{ij}^{(1)}$

x

r

θ

y

θ_1

θ_2

Traction
Free edges

b)

$C_{ij}^{(1)}$

$C_{ij}^{(3)}$

$C_{ij}^{(2)}$

x

r

θ

y

θ_1

θ_2

θ_3

a)

Type I

σ_0

h_1

Adherent

Adhesive

h

h_2

C_1 — l — C_2
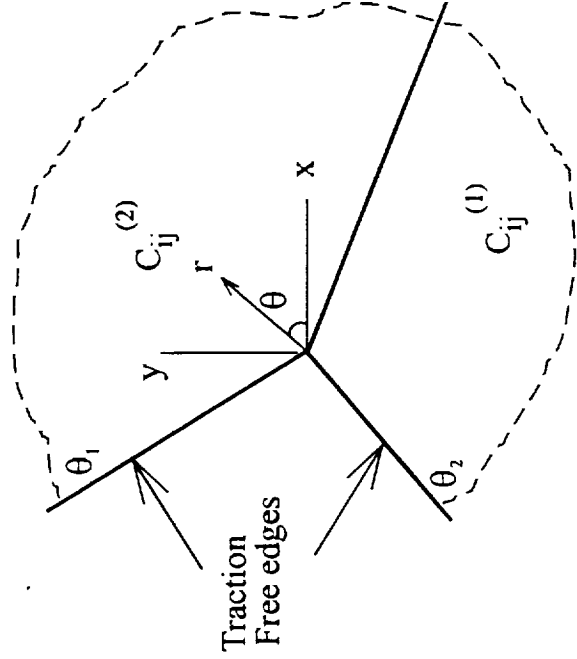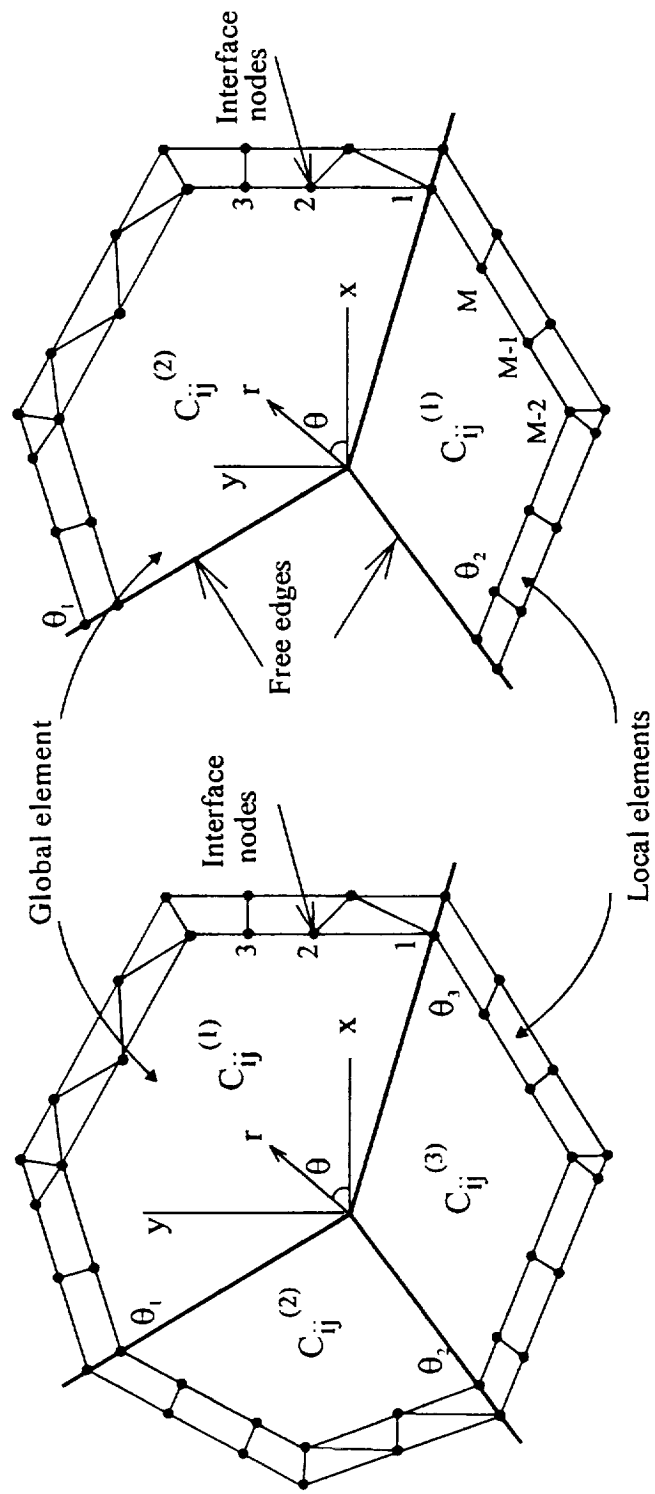
(a) without adhesive overflow

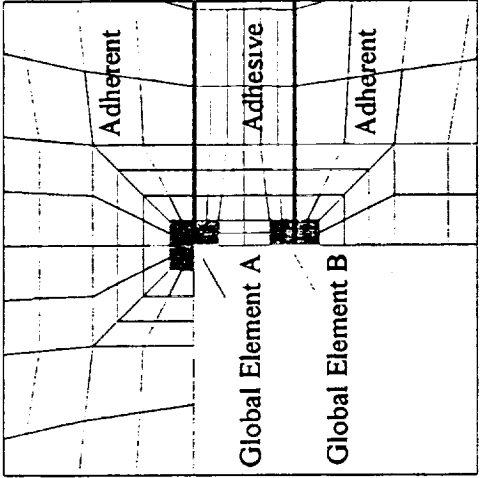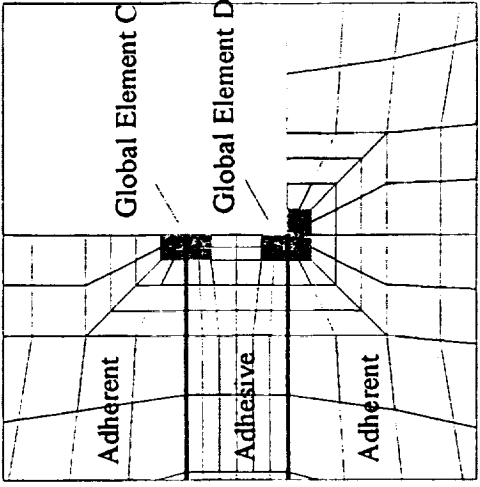Type II

σ_0
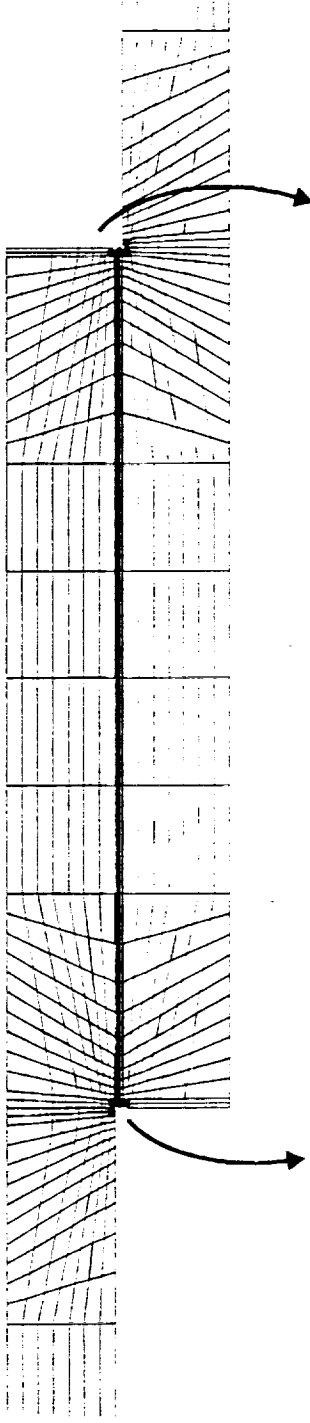
h_1

θ_1

Adherent

Adhesive

θ_2 h

h_2

C_1 — l — C_2

(b) with beveled adherents

Type III

σ_0

h_1 l_1

Adherent

Adhesive

ϕ_1

ϕ_2

h

l_2 h_2

C_1 — l — C_2
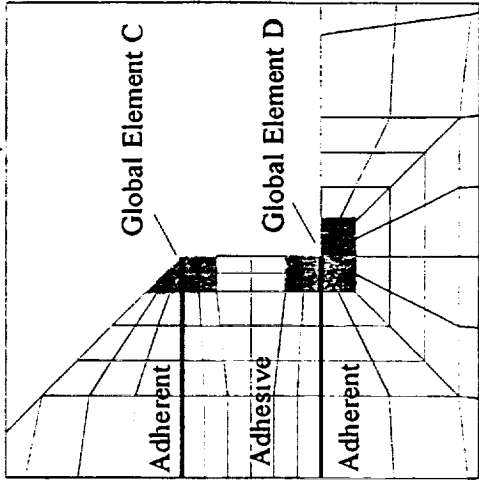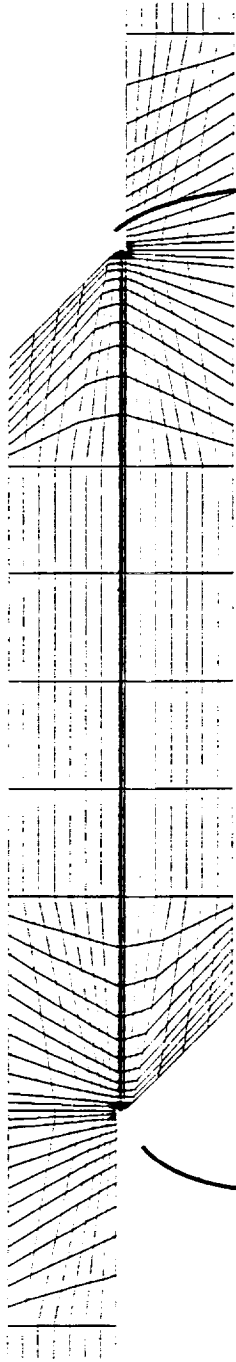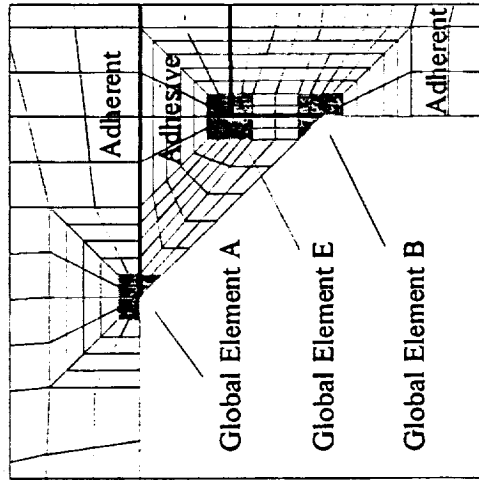
(c) with adhesive overflow

Global Element C

Global Element D

Adherent

Adhesive

Adherent

Adherent

Adhesive

Adherent

Global Element A

Global Element B

Global Element C

Global Element D

Adherent

Adhesive

Adherent

Adherent

Adhesive

Adherent

Global Element A

Global Element B

Global Element C
Global Element F
Global Element D

Adhesive
Adherent
Adherent

Adherent
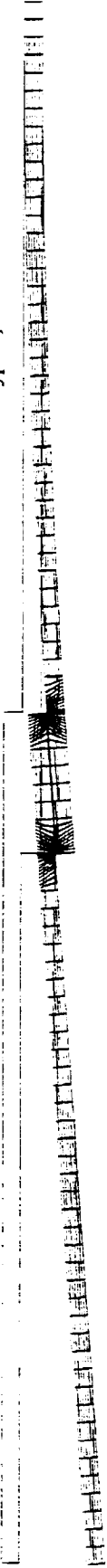Adhesive

Adherent

Global Element A
Global Element E
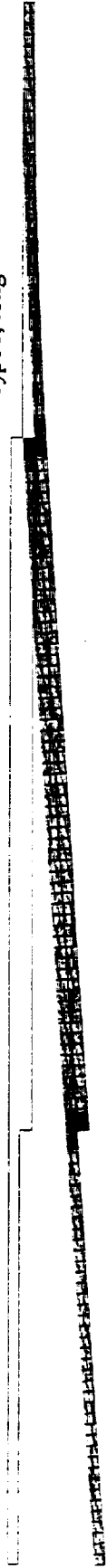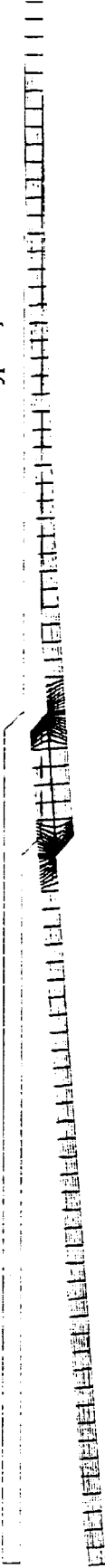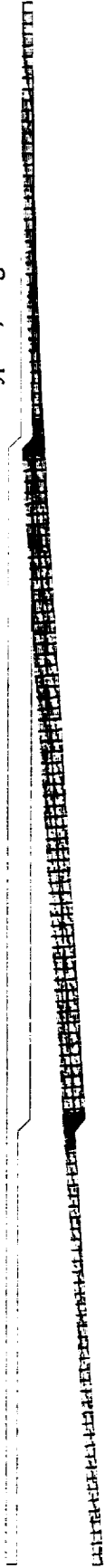Global Element B

Type 1, short

Type 1, long

Type 2, short

Type 2, long

Type 3, short

Type 3, long

Global Element A

Global Element B

Global Element C

Global Element D

Global Element A

1E-5

Stresses, MPa

1.2
1
0.8
0.6
0.4
0.2
0
-0.2
-0.4
-0.6

7
6
5
4
3
2
1
0

Strain energy density, S

S

σ_ϑ

$\tau_{r\vartheta}$

Adhesive

Adherent

-100   -50   0   50   100   150

θ, deg.

Global Element A

Global Element B

1E-6

Stresses, MPa

0.15

0.1

0.05

0

-0.05

-0.1

16
14
12
10
8
6
4
2
0

Strain energy density, S

$\tau_{r\vartheta}$

S

σ_ϑ

Adherent

Adhesive

-40   -20   0   20   40   60   80

θ, deg.

Global Element B

Global Element C

Global Element D

Global Element A

Global Element B

Global Element C

Global Element D

Global Element E

Global Element F